

Evidence for nano-scale inhomogeneities in bilayer manganites in the Mn⁴⁺ rich region: $0.54 \leq x \leq 0.80$

Xiangyun Qiu and Simon J. L. Billinge

Department of Physics and Astronomy and Center for Fundamental Materials Research, Michigan State University, Biomedical Physical Sciences, East Lansing, MI 48824-2320.

Carmen R. Kmetz and John F. Mitchell

Material Science Division, Argonne National Laboratory, 9700 S Cass Avenue, Argonne, Illinois, 60439

(Dated: November 20, 2018)

The atomic pair distribution function (PDF) technique is employed to probe the atomic local structural responses in naturally double layered manganites $\text{La}_{2-2x}\text{Sr}_{1+2x}\text{Mn}_2\text{O}_7$ in the doping range $0.54 \leq x \leq 0.80$. Our low temperature neutron powder diffraction measurements suggest the coexistence of two different Jahn-Teller (JT) distorted MnO_6 octahedra when its ordered magnetic structure crosses over from type A ($0.54 \leq x \leq 0.66$) to type C/C* ($0.74 \leq x \leq 0.90$) ordering. At all doping levels at low temperature the doped holes reside predominantly in the plane of the bilayer. In the type A magnetic ordering regime, the e_g electrons appear to be significantly delocalized in the plane resulting in undistorted octahedra, while in type C/C* regime, elongated JT distorted octahedra are apparent. This is consistent with the presence of inhomogeneous coexisting delocalized and localized electronic states. No evidence of macroscopic phase separation has been observed. Such nanoscale inhomogeneities may explain the magnetically frustrated behavior observed in the spin disordered “gap” region ($0.66 \leq x \leq 0.74$).

PACS numbers: 61.12.-q, 75.47.Lx, 75.47.Gk

I. INTRODUCTION

The double layered manganite series $\text{La}_{2-2x}\text{Sr}_{1+2x}\text{Mn}_2\text{O}_7$ shows a rich and interesting, but somewhat poorly understood, phase diagram.^{1,2} It also appears to be a prospective candidate for future application by showing a large colossal magnetoresistance (CMR) effect.³ The interplay between spin, charge, and lattice degrees of freedom is of critical importance to many transitional-metal oxides with perovskite-related structures, and their delicate interactions have been intensely studied both theoretically and experimentally. The reduced dimensionality obtained by constraining the lattice degree of freedom in this bi-layered system facilitates the investigation of strong correlation between electron-lattice coupling and magnetic properties, proving it to be one of the most interesting CMR manganites.

Most studies focus on the Mn³⁺ rich portion of the $\text{La}_{2-2x}\text{Sr}_{1+2x}\text{Mn}_2\text{O}_7$ phase diagram, where the important CMR phenomenon and the temperature driven Insulator-Metal (IM) transition are observed.³ However, the phase diagram of the less studied Mn⁴⁺ rich region shows many novel and intriguing properties.² For convenience, this is reproduced in Fig. 1. For example, the type-A anti-ferromagnetic insulator (AFI) phase is the ground state in a wide range $0.46 \leq x \leq 0.66$ while it is more commonly found in cubic manganites at the lowest Sr²⁺ dopings, though with some exceptions.^{4,5} Also, a spin disordered “gap” region takes over for doping x from 0.66 to 0.74; then a tetragonal to orthorhombic crystallographic phase transition occurs sharply at $x=0.74$,

followed by the type C/C* AFI phase up to 0.90 doping. There is also a wide charge ordered (CO) region ($0.48 \leq x \leq 0.66$). These observations challenge the simple Goodenough-Kanemori (GK) rules⁶ that successfully correlate the magnetic and structural properties of cubic perovskite manganites and are not well understood.

An A-type AFI phase, of ferromagnetic sheets antiferromagnetically coupled, at 50% doping can be explained within the framework of the GK rules if the Mn $3d_{x^2-y^2}$ orbitals are occupied by the e_g electrons rather than the more commonly observed $3d_{3y^2-r^2}$ occupancy. However, to explain the C/C* AFI phase (linear FM coupled chains that are antiferromagnetically coupled to their neighbors) at high doping requires $3d_{3y^2-r^2}$ occupancy. Because of the symmetry of these different orbitals the former, $3d_{x^2-y^2}$ occupancy, will result in oblate (two short and four long bonds) and the latter, $3d_{3y^2-r^2}$ occupancy, in prolate (two long, four short bonds) JT-distorted octahedra. Alignment of the long-bonds in the plane along the b -axis naturally explains the observed orthorhombic symmetry.² In addition, a theoretical model based on the two e_g orbitals by Okamoto *et al.*⁷ also suggests the stabilization of $3d_{x^2-y^2}$ and $3d_{3y^2-r^2}$ orbitals in type A and type C/C* magnetic phases respectively.

One outstanding question is the origin of the wide spin disordered region ($0.66 \leq x \leq 0.74$). Because of the change in symmetry of the occupied orbitals a transition from A- to C/C*-type order must be first order. Presumably in the spin disordered region a competition exists between these two magnetic orders that frustrates the system preventing magnetic long-range order from forming. It would be interesting to study the local spin corre-

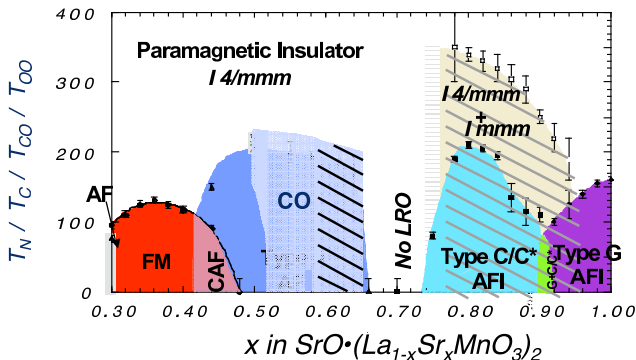


FIG. 1: Structural and magnetic phase diagram of the bilayer manganite $\text{La}_{2-2x}\text{Sr}_{1+2x}\text{Mn}_2\text{O}_7$ in the range $0.3 \leq x \leq 1.0$ determined by neutron powder diffraction. Solid markers represent the magnetic transition temperature (T_C or T_N); open squares delineate the tetragonal to orthorhombic transition. Several magnetic phases are identified: ferromagnetic metal (FM), canted antiferromagnetic (CAF), and A-, C-, and G-type antiferromagnetic insulators (AFI). The region marked "No LRO" has no magnetic diffraction peaks at $T \geq 5$ K. Samples in the region marked "CO" exhibit long-range charge ordering reflections in X-ray and/or electron diffraction. A temperature range schematically indicated by the yellow square shows how this long-range charge-ordered state grows then disappears at low temperature.

lations to verify this, but lack of single crystals has, thus far, prevented such studies. However, the local structure can be studied straightforwardly using the atomic pair distribution function (PDF) analysis of neutron powder diffraction data⁸ and the local magnetism can be inferred from this through application of the GK rules.

In the spin-disordered region the crystallographic structure is metrically tetragonal. This would be observed both if the *local* structure is tetragonal and also if it is locally orthorhombic but the locally orthorhombic domains are disordered along the *a* and *b* directions. For example, this would occur if the long bonds of JT-distorted octahedra are randomly arranged along *a* and *b*. The PDF method could distinguish these two cases. Similarly, if Mn^{3+} and Mn^{4+} ions are spatially disordered their presence will be more apparent from a local structural study.⁹

We applied Atomic Pair Distribution Function (PDF) analysis of neutron powder diffraction data to search for the presence of JT distorted MnO_6 octahedra in the doping range $0.54 \leq x \leq 0.80$ at low temperature. Being a high resolution local structure probe, PDF technique has proved to be capable of resolving different levels of MnO_6 octahedra JT distortions in cubic perovskite manganites.⁹ The advantage of this technique is that both Bragg and diffuse scattering intensities are used, reflecting both long and short range structural correlations. This enables us to study local structures contained in diffuse scattering found underneath and between the Bragg peaks.⁸

The results indicate a gradual change of the local struc-

ture with doping rather than an abrupt phase transition as seen in the average structure. Local orthorhombicity is evident as early as $x = 0.60$ where the average structure is clearly tetragonal. This supports the idea that the sample is inhomogeneous on the nano-scale with $3d_{x^2-y^2-r^2}$ symmetry JT distorted Mn^{3+} octahedra coexisting with undistorted Mn^{3+} and Mn^{4+} octahedra. The number of JT distorted octahedra varies smoothly with doping.

II. EXPERIMENTS

Finely powdered samples of $\text{La}_{2-2x}\text{Sr}_{1+2x}\text{Mn}_2\text{O}_7$ ($x = 0.54, 0.60, 0.64, 0.66, 0.68, 0.70, 0.72, 0.76, 0.78, 0.80$) were synthesized at Argonne National Laboratory (ANL). The synthesis method is described elsewhere.¹⁰ All samples were characterized using x-ray diffraction and susceptibility measurements. The oxygen content was verified by measuring the *c*-axis parameter and was found to fall on the expected curve for stoichiometric samples.

Neutron powder diffraction measurements were carried out on the Special Environment Powder Diffractometer (SEPD) at the Intense Pulsed Neutron Source (IPNS) at ANL. The samples of about 7.0 g were sealed in cylindrical vanadium cans with helium exchange gas. Data were collected at 4 K for all the compounds using a closed cycle helium refrigerator. The $x = 0.64$ and $x = 0.68$ samples were measured four months after the others. Standard corrections were made to the raw data to account for experimental effects such as detector dead time and efficiency, background, sample absorption, multiple scattering to obtain the normalized total scattering structure function, $S(Q)$, where Q is the magnitude of the scattering vector. These procedures are described in detail elsewhere.⁸ All corrections were carried out using the program PDFgetN.¹¹ The PDF, $G(r)$, is obtained by a Fourier transformation according to $G(r) = \frac{2}{\pi} \int_0^\infty Q[S(Q) - 1] \sin Qr dQ$. The PDF gives the probability of finding an atom at a distance r away from another atom. An example of the PDF from $\text{La}_{2-2x}\text{Sr}_{1+2x}\text{Mn}_2\text{O}_7$ ($x = 0.80$) at 4 K is shown in Fig. 2(b) with the diffraction data in the form of $F(Q) = Q[S(Q) - 1]$ in Fig. 2(a). Superimposed on the PDF is a fit to the data of the average structure model using the profile fitting least-squares regression program, PDFFIT.¹² The $S(Q)$ data were terminated at $Q_{max} = 33.0 \text{ \AA}^{-1}$. This is a reasonable value for Q_{max} in typical PDF measurements on SEPD. Uncertainties at the level of σ are drawn as dashed lines on the difference curves.

Peaks in $G(r)$ represent the probability of finding pairs of atoms separated by the distance- r , weighted by the product of the corresponding atom pair's scattering lengths. In a perfect crystalline $\text{La}_{2-2x}\text{Sr}_{1+2x}\text{Mn}_2\text{O}_7$ structure, the nearest neighbor distance comes from the 6 equidistant Mn-O bond lengths in one MnO_6 octahe-

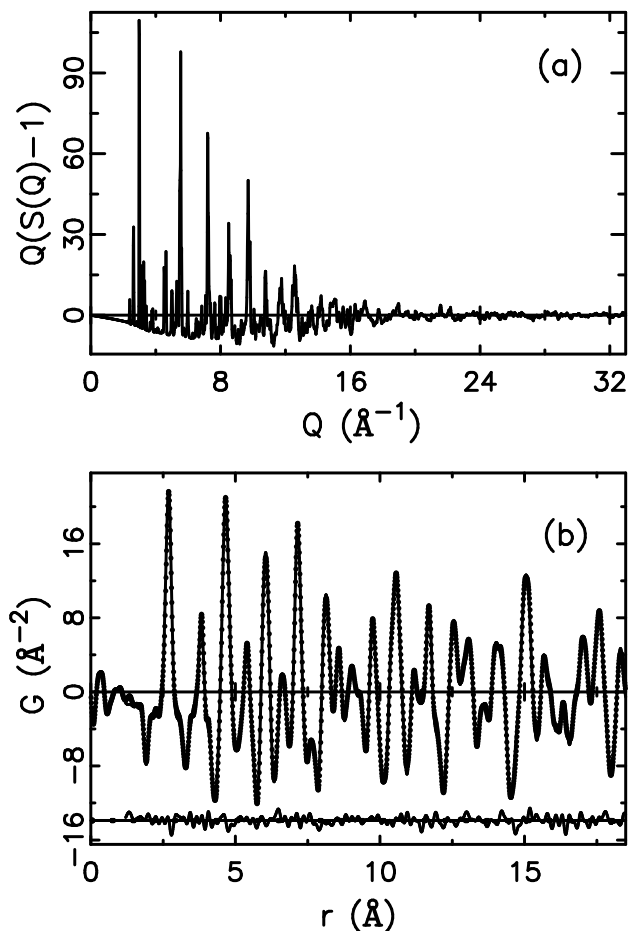


FIG. 2: (a) The experimental reduced structure function $F(Q) = Q*(S(Q)-1)$ of $\text{La}_{2-2x}\text{Sr}_{1+2x}\text{Mn}_2\text{O}_7$ at $x=0.80$. (b) The experimental $G(r)$ obtained by Fourier transforming the data in (a) (solid dots) and the calculated PDF from refined structural model (solid line). The difference curve is shown offset below.

dron, corresponding to the first peak in PDF at about 1.94 Å. This is negative due to Mn atom's negative neutron scattering length. Peaks at higher- r generally contain contributions from more than one unresolved pair. The peak at 2.72 Å is dominated by high multiplicity O-O correlations, though it also contains a contribution from La/Sr-O correlations. The decomposition of multiple contributions is handled by a real space Rietveld refinement program: PDFFIT,¹² with which a structural model can be obtained without the constraints posed by space group symmetries. Therefore, both local structural and average structure analysis can be performed on the same data set.

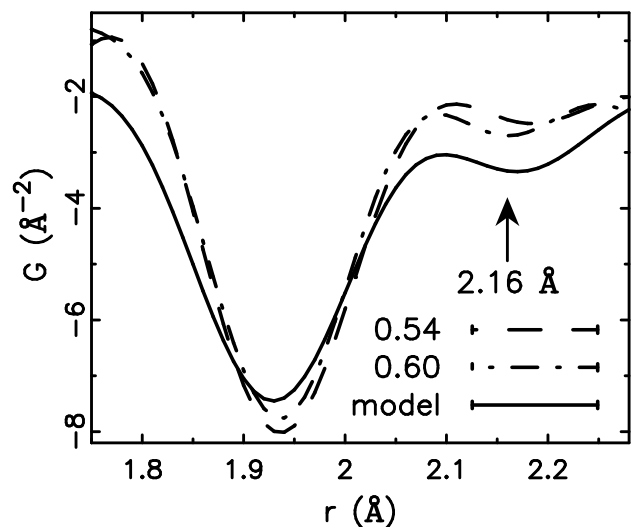


FIG. 3: Two dashed lines show the experimental PDFs of doping x at 0.54 and 0.60. While the model PDF shown as solid line is calculated assuming 46% prolate octahedra (two long Mn-O bonds at 2.16 Å, four short ones at 1.935 Å) mixed with 54% normal octahedra (6 Mn-O bonds at 1.935 Å).

III. RESULTS

A. Model independent analysis

Low- r PDF peaks directly reflect the local structural details, and disorder in the local structure can cause excess peak broadening,⁹ extra shoulders¹³ and even split peaks.¹⁴ The prolate JT distorted octahedra of Mn^{3+} ions result in four short Mn-O bonds in the range 1.92–1.97 Å and two long bonds at 2.16 Å.^{14,15,16} In the cubic manganites, in the absence of disorder, these are easily resolved in the PDF.¹⁴ With doping the loss of orientational order of the orbitals quickly suppresses the coherent JT distortion and the average structure changes from orthorhombic to rhombohedral. However, the presence of fully JT distorted octahedra is evident in the local structure, though the peak in the PDF from the long-bonds is not resolved and is evident only as a broad shoulder.^{9,17,18}

We first investigated the PDFs from these layered, doped, manganites to search for qualitative evidence for the existence of long $r = 2.16$ Å bonds. This is shown in Figs. 3 and 4. Figure 3 shows the experimental PDFs at $x = 0.54$ and 0.60 with a calculated PDF from a model assuming all Mn^{3+}O_6 octahedra are prolate. In this case the number of Mn^{3+} octahedra is determined from the doping and of these, two out of six Mn-O bonds are set to 2.16 Å. The clear discrepancies between experiments and model rule out the existence of fully JT distorted prolate MnO_6 octahedra in the type A AFI phase. As we discuss elsewhere, this is probably due to the fact that electrons are largely delocalized in the planes (though not perpendicular to them) in this region of the phase diagram at

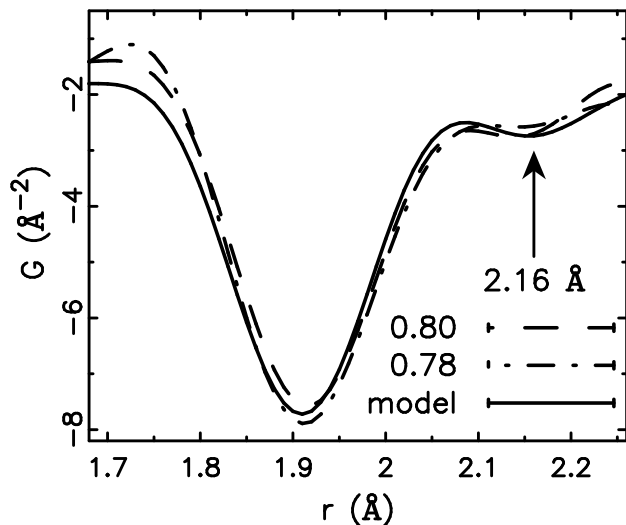


FIG. 4: Two dashed lines show the experimental PDFs of doping x at 0.78 and 0.80. While the model PDF shown as solid line is calculated assuming 20% prolate octahedra (2 long Mn-O bonds at 2.16 Å, 4 short ones at 1.935 Å) mixed with 80% normal octahedra (6 Mn-O bonds at 1.935 Å).

low-T,¹⁹ in analogy with the situation in the CMR region of the cubic manganites.^{9,17,18}

In the type C/C* orthorhombic phase, we expect e_g electrons to stay in $3d_{3y^2-r^2}$ orbitals, and therefore the 2.16 Å long bonds are expected to be present. In this case the number of Mn³⁺ sites, and therefore the number of long-bonds, is rather small. Nonetheless, there is rather good agreement between the prediction of the simple model and the data in the region around $r = 2.16$ Å. Figure 4 shows the experimental PDFs at $x = 0.78$ and 0.80 with the model-PDF. Because of the small number of long bonds (6.7% at $x = 0.8$) this result is not conclusive evidence supporting the existence of these long bonds, though the data are consistent with their presence.

The PDF peaks represent the bond length *distributions* in the material. The proposed MnO₆ octahedral shape change of the Mn³⁺ octahedra, from normal to prolate JT distorted with increasing doping, induces more local structural distortion and thus would cause the low- r PDF peak to broaden. An increase in disorder in the local structure will result in this peak broadening, and therefore lowering, with doping as observed. In Fig. 5 we show the change of the peak height, inversely related to the peak width, of the first PDF peak around 1.935 Å with doping. The $x = 0.64$ and 0.68 samples lie above the others. These samples were measured at a later date and evidently the systematic errors have not been perfectly reproduced. Note that the data were all collected at 4 K so no temperature broadening effects are expected. Also, increasing the doping in this highly doped region moves the composition towards the pure stoichiometric end-member and so dopant ion induced disorder coming from the alloying is decreasing with increasing doping.

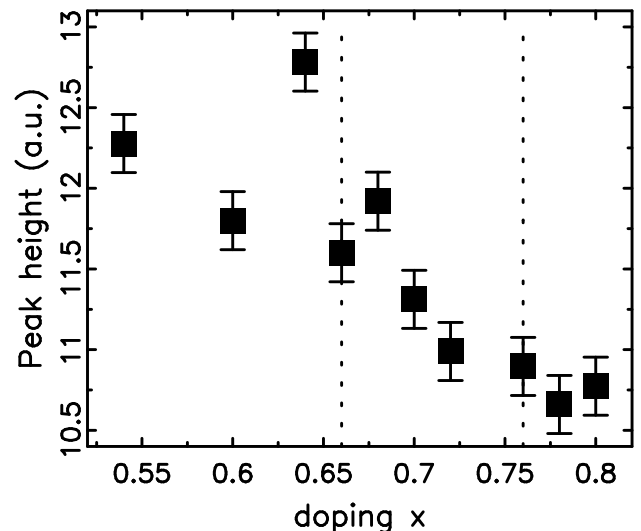


FIG. 5: Solid squares show the magnitudes of the heights of the first Mn-O peak around 1.94 Å. Vertical dotted lines indicate positions of magnetic phase transitions from type-A to spin disordered to type C/C*.

The observation of an increase in disorder with increasing doping, in this peak that is highly sensitive to the Mn-O bonds, is therefore strong evidence that an electronically driven change is occurring in the Mn-O octahedral shape.

The smooth evolution of the peak heights (Fig. 5) suggests that the local structural changes occur continuously with changes of doping concentration x , in contrast to what is observed in the average structure. The change in global symmetry from tetragonal to orthorhombic at $x = 0.76$ is presumably related to a transition of the JT long-bonds from being randomly oriented to having a net orientation along b .

B. Structural Modelling

Structural modelling gives a more quantitative picture of the local structure than the qualitative analysis described above. Two structural models were fit based on the tetragonal and orthorhombic crystallographic models.² It is worth noting here that any constraint by the space group and symmetry during average structure analysis can be relaxed in our real space full profile modelling. Additionally, we can add any kind of constraints based on physical reasons. It was found that the best agreement was found for doping $x \geq 0.60$ when the tetragonal symmetry is relaxed to orthorhombic. In the case of $x = 0.60$ the improvement in fit of the orthorhombic model is barely significant and in this case we cannot unambiguously assign the local symmetry as orthorhombic. In the following, only results from the relaxed orthorhombic symmetry are reported.

The two in-plane lattice constants a and b are shown in Fig. 6 together with the lattice constants obtained from

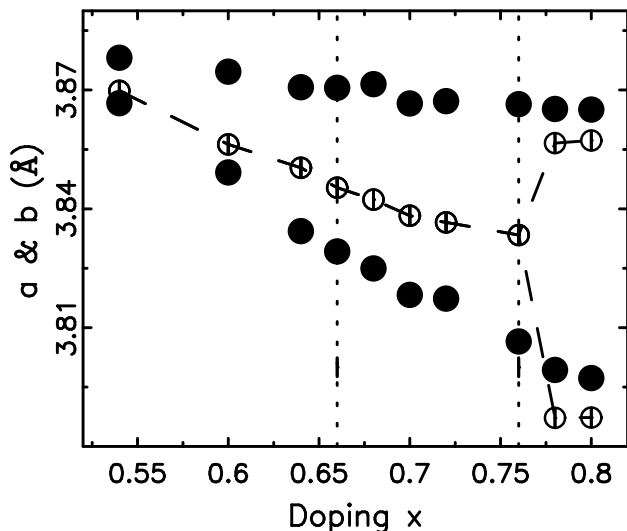


FIG. 6: Solid circles are the in-plane lattice constants a and b from PDF refinements with orthorhombic models, while open circles are from Rietveld refinements on the same data with tetragonal and orthorhombic models in $0.54 \leq x \leq 0.76$ and $0.78 \leq x \leq 0.80$, respectively. Vertical dotted lines indicate positions of magnetic phase transitions from type-A to spin disordered to type C/C^* .

Rietveld refinement using GSAS.²⁰ The two dashed vertical lines show the phase transition from type-A AFI to spin disordered and tetragonal to orthorhombic (which is almost coincident with the magnetic transition from spin disordered to type C/C^* AFI), respectively. The PDF refinements suggest the structure is already locally orthorhombic as early as $x = 0.60$, while the sharp crystallographic phase transition occurs around $x = 0.76$. This could be explained if JT distorted MnO_6 octahedra are beginning to appear on Mn^{3+} sites around $x = 0.60$, but the long bonds lie along the a and b axes randomly.

It is important to determine whether the JT long-bonds that appear at $x \geq 0.60$ lie in the plane, perpendicular to the plane, or are distributed between these possibilities. This can be studied by looking at the refined values of the Mn-O bond lengths. The four different Mn-O bond lengths within one MnO_6 octahedron, determined by PDFFIT, are shown in Fig. 7. What is clear from this Figure is that over this doping range there is no clear trend in the apical (perpendicular) bonds. This implies that the observed increase in the Mn-O bond-length distribution with doping is coming primarily from the in-plane bonds. The JT distorted Mn^{3+} ions that appear with doping are predominantly locating their long-bonds in the plane. The electronic states along c remain largely unchanged with doping, and little or no charge transfer occurs between in-plane and out of plane.

We have observed evidence for JT long bonds lying in the plane from the PDF refinements. If this picture is correct we would expect to see a response in the refined in-plane Mn and O displacement factors. These should

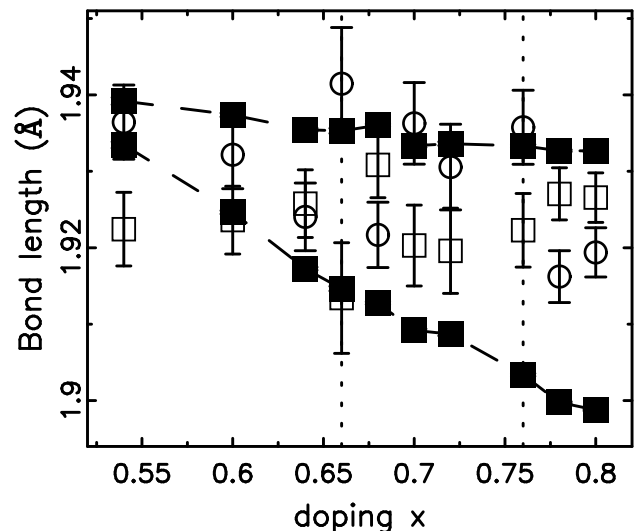


FIG. 7: Solid squares are the two in-plane (ab) Mn-O bond lengths. The bond length between Mn and the out of plane O atom is shown as open squares, while the bond length between Mn and the intra plane O atoms is shown as open circle. Vertical dotted lines indicate positions of magnetic phase transitions from type-A to spin disordered to type C/C^* .

be small for $x < 0.60$ because there is little disorder in the structure and the models that we are using, based on the average structure, should work well also for the local structure. We might expect them also to be small and largely thermal in origin for $x > 0.76$ where the JT distorted orbitals are ordered along the b axis. In the spin disordered region we see evidence in the local structure for significant numbers of JT distorted Mn^{3+} ions that are not fully ordered. By allowing the local structure to be orthorhombic much of this disorder will not show up in PDF derived displacement factors. However, it is interesting to note that there is a peak in the value of the planar Mn-O displacement parameters in this region, as shown in Fig. 8.

IV. DISCUSSION

In a separate article we present the evidence supporting the fact that, at low temperature at $x = 0.54$, the e_g electrons associated with Mn^{3+} ions are delocalized in the plane. At this point there are no JT distorted MnO_6 octahedra and the local structure agrees with the average structure. When the C/C^* -type antiferromagnetism appears around $x = 0.76$, coincident with a global orthorhombic distortion, it seems clear that JT distorted MnO_6 octahedra have appeared with the $3d_{3y^2-r^2}$ orbitals occupied. The main result from the current work is the observation that, in the local structure, the crossover between these two behaviors happens continuously with doping and is not abrupt as it is in the average structure. The structure is locally orthorhombic as early as

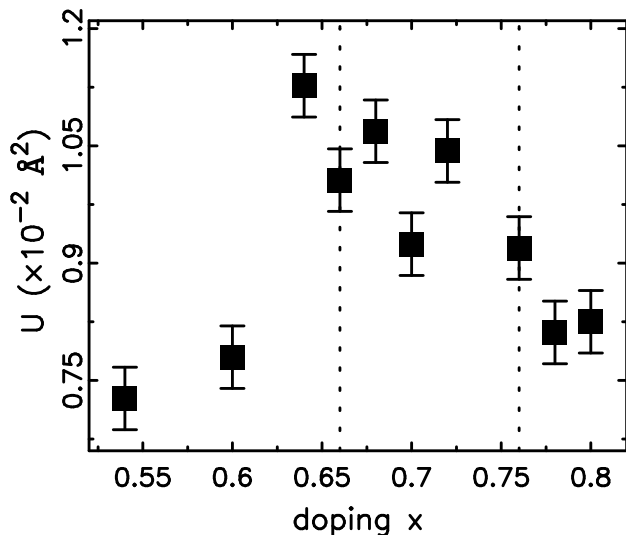


FIG. 8: Thermal displacement factor of the in-plane O atoms along the direction of Mn-O bonds. Vertical dotted lines indicate positions of magnetic phase transitions from type-A to spin disordered to type C/C*.

$x = 0.60$ suggesting the presence of JT distorted MnO_6 octahedra that are orientationally disordered within the plane. From this work we cannot tell if this disorder is static or dynamic.

This picture could qualitatively explain the spin-disordered region since, from the GK rules, local magnetic correlations will randomly fluctuate between ferromagnetic and antiferromagnetic from site to site.

More detailed consideration of this model suggests that the sample is likely to be nano-phase segregated in this region since we believe the low-doping end-member (the $x = 0.54$ sample) has its e_g electrons delocalized in the plane.²¹ For this to make sense, delocalized clusters with locally A-type magnetic correlations must persist in this spin disordered region. Since there is no evidence of macroscopic phase-separation these clusters are likely to be nano-scale. Presumably they coexist with nanoscale regions of the sample where the e_g electrons are localized as Mn^{3+} ions with a local JT distortion. With increasing doping the number of these localized Mn^{3+} sites first increases as the proportion of the sample in the localized state increases at the expense of the delocalized state. Once the entire sample has transformed to the localized

state, with increasing doping the number of Mn^{3+} sites will decrease as $(1-x)$ in the normal way. This is apparent from the decreasing orthorhombicity that is evident for $x > 0.80$.²

V. CONCLUSIONS

Based on PDF results, we suggest that the local structure of $\text{La}_{2-2x}\text{Sr}_{1+2x}\text{Mn}_2\text{O}_7$ evolves smoothly as a function of doping at low temperature in the region of the phase diagram $0.54 \leq x \leq 0.80$. The material evolves smoothly from being locally tetragonal at $x = 0.54$ to having a well established orthorhombicity at $x = 0.80$. The local and global structures agree well at these end-points. However, in between, and associated with the spin disordered region of the phase diagram, the local structure appears orthorhombic even though the material is metrically tetragonal. These results can be reconciled if JT distorted MnO_6 octahedra exist with their long-bonds lying in the plane but disordered along the a and b axes. We have discussed that these results are consistent with the presence of inhomogeneities resulting in a coexistence of delocalized and localized electronic states, possibly due to nano-scale phase separation, in this intermediate region of the phase diagram, into regions that have the characteristics of the two end-members at $x = 0.54$ and $x = 0.80$ respectively. We have argued that such a nano phase separation into disordered and possibly fluctuating A-type and C/C*-type magnetic domains may explain the frustrated magnetism in this region. Making certain assumptions we have quantified the evolution of the phase separation with doping.

Acknowledgments

We are thankful to Simine Short for providing valuable help with the neutron diffraction data collection. The work at MSU was supported by NSF through grants DMR-0075149, and at ANL by the US Department of Energy, Office of Science, under Contract No. W-31-109-ENG-38. The IPNS at Argonne National Laboratory is funded by the US Department of Energy under contract W-31-109-ENG-38.

¹ M. Kubota, H. Fujioka, K. Ohoyama, K. Hirota, Y. Moritomo, and H. Yoshizawa, *J. Phys. Chem. solids* **60**, 1161 (1999).

² C. D. Ling, J. E. Millburn, J. F. Mitchell, D. N. Argyriou, and J. Linto, *Phys. Rev. B* **62**, 15096 (2000).

³ Y. Moritomo, Y. Tomioka, A. Asamitsu, Y. Tokura, and Y. Matsui, *Nature (London)* **141**, 380 (1996).

⁴ Y. Moritomo, T. Akimoto, A. Nakamura, K. Ohoyama,

and M. Ohashi, *Phys. Rev. B* **58**, 5544 (1998).

⁵ H. Kuwahara, T. Okuda, Y. Tomioka, A. Asamitsu, and Y. Tokura, *Phys. Rev. Lett.* **82**, 4316 (1999).

⁶ J. B. Goodenough, *Phys. Rev.* **100**, 564 (1955).

⁷ S. Okamoto, S. Ishihara, and S. Maekawa, *Phys. Rev. B* **63**, 104401 (2001).

⁸ T. Egami and S. J. L. Billinge, *Underneath the Bragg Peaks: Structural analysis of complex materials*, Pergamon

- Press, Oxford, England, 2003, to be published.
- ⁹ S. J. L. Billinge, R. G. DiFrancesco, G. H. Kwei, J. J. Neumeier, and J. D. Thompson, *Phys. Rev. Lett.* **77**, 715 (1996).
- ¹⁰ J. E. Millburn, J. F. Mitchell, and D. N. Argyriou, *Chem. Commun.* **3**, 1389 (1999).
- ¹¹ P. F. Peterson, M. Gutmann, Th. Proffen, and S. J. L. Billinge, *J. Appl. Crystallogr.* **33**, 1192 (2000).
- ¹² Th. Proffen and S. J. L. Billinge, *J. Appl. Crystallogr.* **32**, 572 (1999).
- ¹³ D. Louca, G. H. Kwei, and J. F. Mitchell, *Phys. Rev. Lett.* **80**, 3811 (1998).
- ¹⁴ Th. Proffen, R. G. DiFrancesco, S. J. L. Billinge, E. L. Brosha, and G. H. Kwei, *Phys. Rev. B* **60**, 9973 (1999).
- ¹⁵ J. B. A. A. Elemans, B. Van Laar, K. R. Van Der Veen, and B. O. Loopstra, *J. Solid State Chem.* **3**, 238 (1971).
- ¹⁶ J. Rodríguez-Carvajal, M. Hennion, F. Moussa, A. H. Moudden, L. Pinsard, and A. Revcolevschi, *Phys. Rev. B* **57**, R3189 (1998).
- ¹⁷ S. J. L. Billinge, Th. Proffen, V. Petkov, J. Sarrao, and S. Kycia, *Phys. Rev. B* **62**, 1203 (2000).
- ¹⁸ S. J. L. Billinge, in *Intrinsic Multiscale Structure and Dynamics of Complex Electronic Oxides*, edited by S. Shenoy and A. R. Bishop, pages to be published. See cond-mat/0210559, Singapore, 2003, World Scientific.
- ¹⁹ X. Qiu, S. J. L. Billinge, J. F. Mitchell, and C. R. Kmetz, (2003), unpublished.
- ²⁰ A. C. Larson and R. B. Von Dreele, General structure analysis system, Report No. LAUR-86-748, Los Alamos National Laboratory, Los Alamos, NM 87545, 1987.
- ²¹ K. E. Gray and J. F. Mitchell, unpublished.